J. Fluid Mech. (1985), vol. 150, pp. 451–465
Printed in Great Britain

Square-pattern convection in fluids with strongly temperature-dependent viscosity

By F. H. BUSSE AND H. FRICK

Department of Earth and Space Sciences and Institute of Geophysics and Planetary Physics, University of California, Los Angeles, California 90024

(Received 16 March 1984 and in revised form 18 July 1984)

Three-dimensional numerical solutions are obtained describing convection with a square lattice in a layer heated from below with no-slip top and bottom boundaries. The limit of infinite Prandtl number and a linear dependence of the viscosity on temperature are assumed. The stability of the three-dimensional solutions with respect to disturbances fitting the square lattice is analysed. It is shown that convection in the form of two-dimensional rolls is stable for low variations of viscosity, while square-pattern convection becomes stable when the viscosity contrast between upper and lower parts of the fluid layer is sufficiently strong. The theoretical results are in qualitative agreement with experimental observations.

1. Introduction

Convection in fluid layers with strong variations of the viscosity has received considerable attention in recent years because of its importance in the thermal history of the terrestrial planets. The strong temperature dependence of solid-state creep is responsible for the large variations of the effective viscosity in the flow of the Earth's mantle. As has often been emphasized (Tozer 1967), the temperature dependence of viscosity governs the effectiveness as a function of temperature of the convective heat transport and thereby the physical state of the Earth's interior. The desire to understand the phenomenon of seafloor spreading and continental drift on the basis of models for mantle convection has led to numerous studies of convection in fluids with strongly temperature-dependent viscosity.

Early theoretical work on weakly nonlinear convection (Palm 1960; Segel & Stuart 1962; Busse 1962, 1967) has demonstrated that the onset of convection occurs in the form of hexagonal cells when material properties such as viscosity vary slightly throughout the convection layer owing to their temperature dependence. When this variation is sufficiently small, hexagonal convection is replaced by convection in the form of rolls as soon as the Rayleigh number is increased by a small amount beyond its critical value. The results are in qualitative agreement with the experimental observations of convection patterns in fluids with temperature-dependent viscosity (Silverston 1958; Somerscales & Dougherty 1970; Hoard, Robertson & Acrivos 1970). In particular the property that the sign of motion in the hexagonal cells depends on the sign of temperature dependence of viscosity was demonstrated experimentally (Tippelskirch 1956). Detailed quantitative measurements of the transition from hexagons to rolls and the transition from rolls to hexagons (which occurs at a different Rayleigh number because of hysteresis effects) have recently been reported by Walden & Ahlers (1981).

The perturbation methods employed in the early work are no longer suitable when

strong variations of viscosity in the fluid layer must be considered. Motivated by the problem of mantle convection, a considerable number of cases of convection in fluids with strongly temperature-dependent viscosity have been investigated numerically. Because of the high computational expenses, however, the numerical solutions have been limited to the two-dimensional case in general (Foster 1969; Torrance & Turcotte 1971; Houston & DeBremaecker 1975; DeBremaecker 1977; Kopitzke 1979; Schmeling & Jacoby 1981; Jacoby & Schmeling 1982). While the two-dimensional computations capture many of the characteristic features introduced by a strongly temperature-dependent viscosity such as the stagnant lid of highly viscous fluid near the top boundary and the asymmetry between up- and downgoing flow, these features will undoubtedly be influenced and modified by the three-dimensional structure of the physically realistic convection flow. The need for a better understanding of the three-dimensional properties of convection with strongly temperature-dependent viscosity has been the primary motivation for the work reported in this paper.

Considerable progress has been made in the experimental investigation of the effects of strong viscosity variations on convection. Surprisingly this effect has been found to be much weaker than expected. Booker (1976) has shown that in the case of nearly exponential variation of viscosity with temperature the onset of convection and the heat transport follow closely the predictions for a constant-viscosity fluid if the Rayleigh number is based on the viscosity corresponding to the arithmetic mean of the temperatures at the two boundaries. Richter (1978) has demonstrated that the transition from two-dimensional to bimodal convection occurs in a fashion similar to that observed in the constant-viscosity experiments of Busse & Whitehead (1971). The secondary component of bimodal convection occurs primarily in the low-viscosity part of the layer, and the critical Rayleigh number for the transition is lowered. These results have been confirmed by the experimental observations of Oliver & Booker (1983) and White (1984). A new phenomenon in the form of square-pattern convection appears, however, when the viscosity contrast between upper and lower boundaries of the layer exceeds a value of order ten (Oliver & Booker 1983; White 1984). It is difficult to determine the points of transitions between the different patterns of rolls, hexagonal and square cells, and bimodal convection in the parameter space and it has become evident that at least the first three patterns can coexist in certain regions of the parameter space. In addition, the different liquids used by different authors complicate the comparison of the results. But the picture emerging from the various laboratory observations is fairly consistent in showing that squares replace rolls and hexagons as the predominant form of convection at moderate Rayleigh numbers when viscosity variations are sufficiently large.

In this paper square-pattern convection in the form of rolls are studied together with the problem of transition from one form to the other in the case when the viscosity depends linearly on temperature. This particular functional dependence is not very realistic as far as the experiments are concerned, and it has been chosen primarily for mathematical convenience; but it permits arbitrarily high ratios r between the viscosities at the upper and lower boundaries. This latter parameter appears to be of primary importance in describing the observations, and it is expected that the theory is capable of describing at least qualitatively all features of physical interest. An infinite Prandtl number is assumed since all experiments have been carried out with high-Prandtl-number fluids. The numerical method is based on a Galerkin expansion of all dependent variables in terms of functions satisfying the boundary conditions. Steady solutions of the basic nonlinear equations are obtained by a

Newton–Raphson iteration. The computer program used for the present problem is an extension of the program used for the earlier analysis of bimodal convection in constant-viscosity fluids (Frick, Busse & Clever 1983). The main shortcoming of the analysis presented in this paper is the omission of solutions describing hexagonal convection. Because of the different structure of this form of convection, major changes in the computer code would have been required. In terms of computational efficiency it seems advisable to study hexagonal convection in connection with a more general approach to the problem of three-dimensional convection which is planned for future development. Since square-pattern convection takes over the role of hexagonal convection to some extent as the viscosity contrast of the layer increases, the competition between squares and rolls appears to be of primary theoretical interest.

The description of the analysis is divided into three major parts. In §2 the mathematical formulation of the problem is given and the method for generating approximate solutions is described. Results for steady two- and three-dimensional convection fitting the horizontal square lattice are discussed in §3. The stability of the steady solutions is investigated and compared with experimental observations in §4. The paper closes with some general remarks in §5.

2. Mathematical description of the problem

We consider a horizontal fluid layer of thickness d with the temperatures T_1 and T_2 prescribed at the upper and lower boundaries respectively. Except for the temperature dependence of the dynamic viscosity

$$\mu = \mu_0[1-\gamma(T-\tfrac{1}{2}(T_2+T_1))], \tag{2.1}$$

the Boussinesq approximation will be assumed in which all material properties are regarded as constant and the small temperature dependence of the density is taken into account in the gravity term only. Using d, d^2/κ and $(T_2-T_1)/R$ as scales for length, time and temperature, the dimensionless equations for the velocity vector u_i and deviation θ of the temperature from the static state can be written in the form

$$\partial_j[(\partial_j u_i+\partial_i u_j)\mu/\mu_0]+\lambda_i\theta-\partial_i p = P^{-1}(u_j\partial_j u_i+\partial_t u_i), \tag{2.2a}$$

$$\partial_j u_j = 0, \tag{2.2b}$$

$$\partial_j\partial_j\theta+R\lambda_j u_j = u_j\partial_j\theta+\partial_t\theta, \tag{2.2c}$$

where the Rayleigh number R and the Prandtl number P are defined by

$$R = \frac{\rho\beta(T_2-T_1)gd^3}{\kappa\mu_0}, \quad P = \frac{\mu_0}{\kappa\rho}, \tag{2.3}$$

and where κ denotes the thermal diffusivity, ρ is the density, β is the coefficient of thermal expansion and g is the acceleration due to gravity. The unit vector λ_i points in the direction opposite to gravity and coincides with the z-axis of a Cartesian system of coordinates. The symbols ∂_i denote differentiation with respect to the coordinates $x_1 = x$, $x_2 = y$, $x_3 = z$, and ∂_t indicates differentiation with respect to time. Assuming that the origin of the coordinate system is located on the midplane of the layer, the boundary conditions at the rigid upper and lower boundaries can be written in the form

$$u_x = u_y = u_z = \theta = 0 \quad \text{at } z = \pm\tfrac{1}{2}. \tag{2.4}$$

In order to obtain steady solutions of (2.2) we introduce the general representation

$$u_i = \delta_i \phi + \varepsilon_i \psi \equiv \epsilon_{ijk} \epsilon_{klm} \lambda_m \partial_j \partial_l \phi + \epsilon_{ijk} \lambda_k \partial_j \psi \tag{2.5}$$

for a solenoidal vector field, where ϵ_{ijk} is the alternator of rank three. By operating with δ_i and ε_i on (2.2a), the following two scalar equations for the fields ϕ and ψ are obtained:

$$\delta_i[(1+\eta z)\partial_k \partial_k \delta_i \phi + \eta \partial_k \lambda_k \delta_i \phi] + \delta_i \lambda_i \theta - \delta_i \partial_j \left\{\frac{\eta\theta}{R}[\partial_j(\delta_i \phi + \varepsilon_i \psi) + \partial_i(\delta_j \phi + \varepsilon_j \psi)]\right\} = 0, \tag{2.6a}$$

$$(1+\eta z)\partial_k \partial_k \varepsilon_j \varepsilon_j \psi + \eta \varepsilon_j \varepsilon_j \partial_k \lambda_k \psi - \varepsilon_i \partial_j \left\{\frac{\eta\theta}{R}[\partial_j(\delta_i \phi + \varepsilon_i \psi) + \partial_i(\delta_j \phi + \varepsilon_j \psi)]\right\} = 0, \tag{2.6b}$$

where the parameter η is defined by

$$\eta = \gamma(T_2 - T_1). \tag{2.7}$$

For the presentation of the results it is convenient to express η in terms of the ratio r between the viscosity at the upper and the viscosity at the lower boundary:

$$\eta = 2(r-1)/(r+1), \tag{2.8}$$

i.e. η increases from the value zero for a fluid of constant viscosity to the value 2 in the limit of an infinite variation of the viscosity between the boundaries. Assuming the limit of infinite Prandtl number, we have neglected the right-hand side of (2.2a). It is of interest to note that the equations (2.6a, b) for ϕ and ψ become decoupled when the viscosity is a function of z only. The nonlinearity introduced into the problem by the dependence of μ on θ is responsible for the generation of vertical vorticity: without this dependence the convective motion is described solely by $\delta_i \phi$ in the limit of infinite Prandtl number and does not exhibit a vertical component of vorticity.

Three-dimensional solutions of (2.2c) and (2.6) can be obtained by expanding ϕ, ψ and θ in terms of systems of orthogonal functions:

$$\phi = \sum_{lnm} a_{lmn} \cos l\alpha_1 x \cos n\alpha_2 y \, g_m(z) \equiv \sum_{lnm} a_{lnm} \Phi_{lnm}, \tag{2.9a}$$

$$\psi = \sum_{lnm} c_{lnm} \sin l\alpha_1 x \sin n\alpha_2 y \, f_m(z) \equiv \sum_{lnm} c_{lnm} \Psi_{lnm}, \tag{2.9b}$$

$$\theta = \sum_{lnm} b_{lnm} \cos l\alpha_1 x \cos n\alpha_2 y \, f_m(z) \equiv \sum_{lnm} b_{lnm} \Theta_{lnm}. \tag{2.9c}$$

The functions

$$g_\nu(z) = \begin{cases} \dfrac{\sinh(\beta_{\frac{1}{2}\nu} z)}{\sinh(\frac{1}{2}\beta_{\frac{1}{2}\nu})} - \dfrac{\sin(\beta_{\frac{1}{2}\nu} z)}{\sin(\frac{1}{2}\beta_{\frac{1}{2}\nu})} & \text{for } \nu \text{ even}, \\ \dfrac{\cosh(\gamma_{\frac{1}{2}(\nu+1)} z)}{\cosh(\frac{1}{2}\gamma_{\frac{1}{2}(\nu+1)})} - \dfrac{\cos(\gamma_{\frac{1}{2}(\nu+1)} z)}{\cos(\frac{1}{2}\gamma_{\frac{1}{2}(\nu+1)})} & \text{for } \nu \text{ odd}, \end{cases} \tag{2.10a}$$

and

$$f_\nu(z) = \sin \nu\pi(z+\tfrac{1}{2}) \tag{2.10b}$$

satisfy the boundary conditions

$$\phi = \frac{\partial}{\partial z}\phi = \theta = \psi = 0 \quad \text{at } z = \pm\tfrac{1}{2} \tag{2.11}$$

for ϕ and for θ or ψ respectively. The values β_v and γ_v are determined as the positive roots of

$$\coth \tfrac{1}{2}\beta - \cot \tfrac{1}{2}\beta = 0, \quad \tanh \tfrac{1}{2}\gamma + \tan \tfrac{1}{2}\gamma = 0,$$

and are given in Chandrasekhar (1961, p. 636). The summations in (2.9) run through $0 \leqslant l, n < \infty$ and $1 \leqslant m < \infty$.

After introducing the representation (2.9) into (2.6) and (2.2*c*), multiplying (2.6*a*), (2.6*b*) and (2.2*c*) by Φ_{ijk}, Ψ_{ijk}, and Θ_{ijk} respectively, and averaging the result over the fluid layer, we obtain a system of algebraic equations for the unknowns a_{lnm}, c_{lnm} and b_{lnm}:

$$L_{km}(i,j)\, a_{ijm} + B_{km}(i,j)\, b_{ijm} + M_{ijklnmpqr}\, a_{lnm}\, b_{pqr} + P_{ijklnmpqr}\, c_{lnm}\, b_{pqr} = 0, \quad (2.12a)$$

$$K_{km}(i,j)\, c_{ijm} + H_{ijklnmpqr}\, a_{lnm}\, b_{pqr} + G_{ijklnmpqr}\, c_{lnm}\, b_{pqr} = 0, \quad (2.12b)$$

$$I_{km}(i,j)\, b_{ijm} R J_{km}(i,j)\, a_{ijm} + N_{ijklnmpqr}\, a_{lnm}\, b_{pqr} + Q_{ijklnmpqr}\, c_{lnm}\, b_{pqr} = 0. \quad (2.12c)$$

The explicit expressions for the matrix elements in these equations are lengthy and will not be given here. We note that considerable simplifications are obtained by partial integration with respect to the operations δ_i, ε_i, ∂_i in front of the curly brackets in (2.6).

For the solution of the system (2.12) of nonlinear algebraic equations by the Newton–Raphson iteration method a truncation must be introduced. The computations reported in the following sections have been done by neglecting all unknowns and corresponding equations with subscripts l, m, n satisfying

$$m + 2(l+n) > N_t, \quad (2.13)$$

where the integer N_t is called the truncation parameter. Other truncation schemes have been tried, but the truncation formula (2.13) appeared to produce the best approximation to the exact solution of the problem for a given number of unknowns when viscosity variations are substantial. Since the truncation formula (2.13) favours the representation of the z-dependence of the solution, it is well suited to approximate the strong vertical dependence of velocity and temperature fields introduced by the varying viscosity.

Because there are no symmetry conditions that reduce the number of non-vanishing coefficients as they do in the constant-viscosity case investigated by Frick *et al.* (1983), the number of coefficients needed for an adequate approximation of the solution is fairly high even at low Rayleigh numbers. Most computations have been done with $N_t = 7$, which yields satisfactorily converged solutions at moderate Rayleigh numbers. The convective heat transport, for example, changes only by 1% typically when $N_t = 8$ is used, unless the Rayleigh number exceeds 3 times its critical value or the viscosity-variation parameter r becomes of order ten or larger. The total number of coefficients for $N_t = 7$ is 90; but this number can be reduced by noting that the coefficients a_{00m}, c_{0nm}, c_{lom} can be replaced by zero since they do not enter (2.12).

3. Steady convection flow

Before discussing the results obtained for two- and three-dimensional convection described by (2.12), it is of interest to inspect the predictions of the linear theory for the problem on hand. The linear analysis of the onset of convection in a fluid with temperature-dependent viscosity has been carried out by a number of authors for a variety of viscosity functions. We refer to the recent paper by Stengel, Oliver & Booker (1982) for a discussion of the different approaches. Since a linear dependence of the viscosity on temperature has not yet been analysed except in the limit of weak

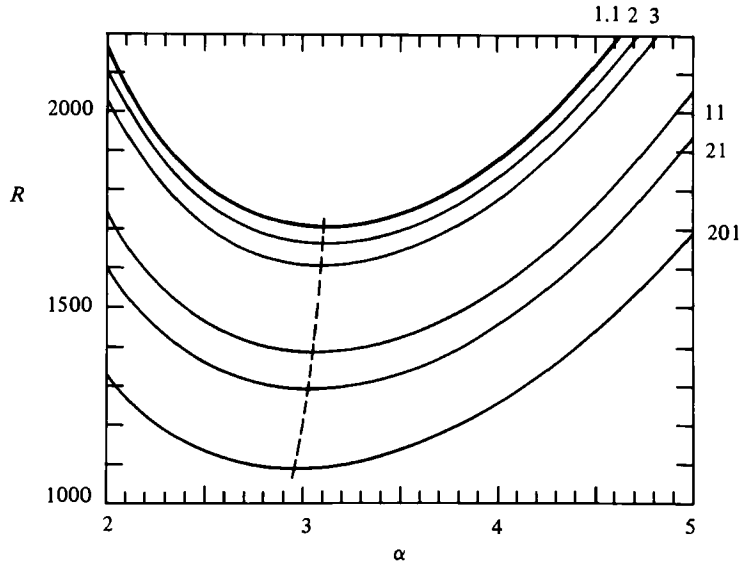

FIGURE 1. The Rayleigh number R computed from the linear equations as a function of the wavenumber α for selected values of the viscosity ratio r.

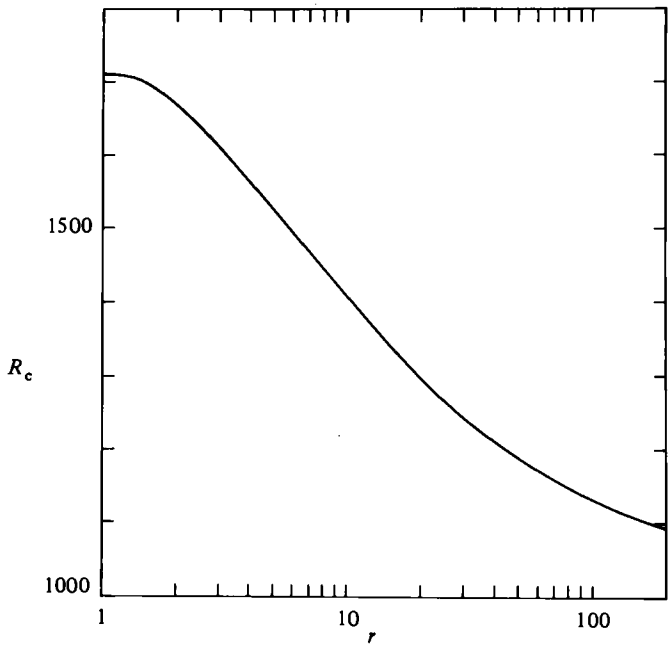

FIGURE 2. The critical Rayleigh number as a function of the viscosity ratio r.

viscosity variation, we present the results of our computations in figures 1 and 2. A Runga–Kutta shooting method has been used to obtain the Rayleigh number as a function of the wavenumber α for different values of r. The results are qualitatively similar to those based on the viscosity function introduced by Palm (1960) and called Palm–Jensen fluid in the work of Stengel *et al.* This viscosity function shares with the relationship (2.1) the property that the viscosity at the median plane of the layer

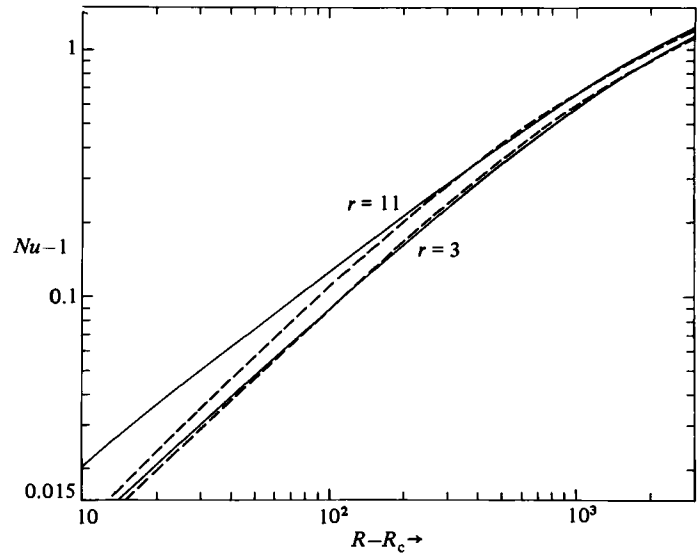

FIGURE 3. The Nusselt number as a function of the Rayleigh number for square-cell convection (solid lines) and for rolls (dashed lines) at two different values of r. The wavenumber $\alpha = 3.1$ has been assumed for all computations. The values $R_c = 1616$ and $R_c = 1408$ for $r = 3$ and 11 have been assumed since they correspond to the values at which the extrapolation of the numerical results indicate vanishing convective heat transport. These values differ slightly from the more accurately determined Runge–Kutta integration results shown in figure 2.

is equal to the average viscosity of the static fluid layer. Thus the critical Rayleigh number R_c decreases with increasing r in figure 2, while R_c typically increases with r, at least initially, for a more realistic exponential dependence of the viscosity on temperature, in which case the average viscosity exceeds the value used in the definition of the Rayleigh number. At very large values of the viscosity ratio r the differences between Palm–Jensen fluids and exponential fluids become quite significant, as Stengel *et al.* point out. For values of r in excess of 10^4 a confinement of the onset of convection to a boundary layer occurs in the exponential fluid, while convection always extends throughout the entire convection layer in the case of a Palm–Jensen fluid or a fluid with a linear dependence of the viscosity on temperature. But for values of r of order 10 which are assumed in the nonlinear computations of the present paper the different viscosity functions mentioned above are not expected to lead to qualitatively different results.

Two- and three-dimensional solutions of (2.12) have been obtained as functions of the Rayleigh number for values of r between 1 and 21. Two-dimensional solutions were generated by dropping equations and coefficients of the system (2.12) with $n > 0$. In the computations of three-dimensional solutions the attention was focused on the square-cell convection case with $\alpha_1 = \alpha_2 = \alpha$. Since the critical wavenumber α does not change much as a function of r, the majority of the computations were carried out for $\alpha = 3.1$ in the two- as well as the three-dimensional case.

In figure 3 the Nusselt number is shown as a function of R for two-dimensional rolls and three-dimensional square cells. There is surprisingly little difference in the heat transport carried by the two forms of convection. The variation of the heat transport with the viscosity ratio r is also rather small if compared at the same value of $R - R_c(r)$. The constant-viscosity case $r = 1$ has not been included in the figure

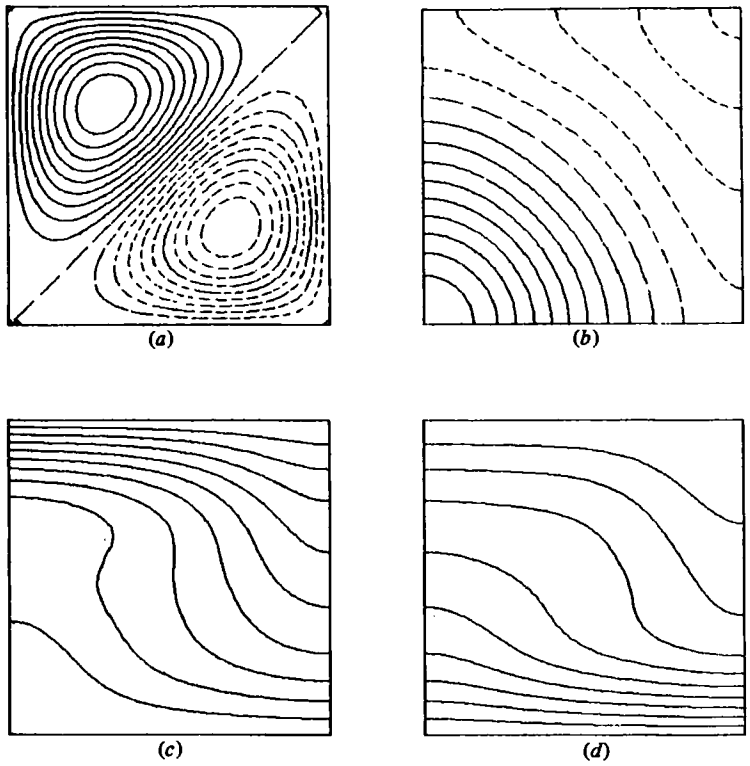

FIGURE 4. Properties of square-cell convection for $R = 4 \times 10^3$, $\alpha = 3.1$, $r = 11$. (*a*) and (*b*) show lines of constant vertical vorticity and constant vertical velocity respectively in the plane $z = 0$. The contours are shown at intervals of $\frac{1}{10}$ of the maximum value; dashed lines indicate negative values. (*c*) and (*d*) show lines of constant temperature in the planes $y = 0$ and $x = \pi/\alpha$.

because the curve for rolls cannot be sufficiently well separated from the curve for $r = 3$. The Nusselt-number–Rayleigh-number dependence in the case $r = 1$ for both rolls and squares is given by Frick *et al.* (1983). For large values of R the heat transported by square-cell convection tends to exceed the heat transport by roll convection. But this property is not caused by the temperature dependence of viscosity; it has also been observed in a fluid of constant viscosity (Frick *et al.* 1983). The increase of the heat transported by square cells in comparison with that carried by rolls at low values of $R - R_c$ is a consequence of the temperature dependence of viscosity. We note that the critical Rayleigh numbers used in figure 3 have been obtained from the Galerkin computations by extrapolation and are thus not as accurate as those obtained by the Runge–Kutta method. But this discrepancy is unlikely to affect the shape of the curves that are plotted in figure 3 as functions of $R - R_c$.

Some properties of the square-cell convection solution can be seen in figure 4. The contours of constant vertical vorticity shown in (*a*) are a special property of convection with temperature-dependent viscosity at infinite Prandtl number. In the limit $r \to 1$ the function ψ and thus the vertical vorticity vanishes. The lines of constant vertical velocity shown in (*b*) indicate the asymmetry between ascending and descending motion which increases with increasing r. In the limit $r \to 1$ this asymmetry vanishes and the contour of vanishing vertical velocity becomes the

diagonal of the square. The asymmetry between rising and descending flow is also seen in (*c*) and (*d*), which show the isotherms within the planes $x = \pi/\alpha$ and $y = 0$. These graphs clearly indicate the strong uplift of the isotherms near the centre, $x = y = 0$, of the convection cell in comparison with the weaker downdraught in the corner, $x = y = \pi/\alpha$, of the cell.

The cellular structure itself is a result of the temperature-dependent viscosity. In the case $r = 1$ the pattern of convection is symmetric in rising and descending motions and cell-like boundaries do not exist. These boundaries develop only as each centre of rising motion become entirely surrounded by a region of descending motion. The resulting structure of the square-convection cells agrees in all qualitative aspects with the square cells seen in the experiments of Oliver & Booker (1983) and White (1984).

4. The pressure distribution

A function which more than any other reflects the influence of varying viscosity, but which is difficult to observe in the laboratory, is the dynamic pressure. The variable p in (2.2*a*) actually describes the dimensionless dynamic pressure, which is defined here as the deviation from the pressure distribution of the static solution of the problem. The role of the ∇p term in the equation of motion is to balance the inhomogeneities in the distribution of the buoyancy force and of viscous stresses and thereby to ensure the continuity of the velocity. Because the stress tensor is a sensitive function of temperature in a fluid with strongly temperature-dependent viscosity, the pressure fields reflects the influence of such a viscosity more directly than does the streamline pattern, for example.

To calculate p it is convenient to take the horizontal divergence of (2.2*a*). Since we are especially interested in the pressure field at the boundary, we find

$$\mu_0 \Delta_2 p \equiv [-\mu \nabla^2 \partial_z u_z - \partial_z \mu \partial_{zz}^2 u_z + \partial_{xz}^2 \mu \partial_z u_x + \partial_{yz}^2 \mu \partial_z u_y] \quad \text{at } z = \pm\tfrac{1}{2}, \tag{4.1}$$

where $\Delta_2 \equiv \partial_{xx}^2 + \partial_{yy}^2$ denotes the horizontal Laplacian. The inspection of the representations (2.5), (2.9) for the velocity field indicates that the pressure at the boundary can be written in the form

$$p(x, y, \pm\tfrac{1}{2}) = \sum_{\kappa,\mu} p_{\kappa\mu}^{(\pm)} \cos \kappa\alpha_1 x \cos \mu\alpha_2 y, \tag{4.2}$$

where the coefficients $p_{\kappa\mu}^{(\pm)}$ satisfy the relationships

$$\begin{aligned} p_{\kappa\mu}^{(\pm)} = \sum_m a_{\kappa\mu m}[g_m'''(\pm\tfrac{1}{2})(1 \pm \eta\tfrac{1}{2}) + \eta g_m''(\pm\tfrac{1}{2})] - \frac{(2-\delta_{x0})(2-\delta_{u0})\eta/R}{(\kappa\alpha_1)^2 + (\mu\alpha_2)^2} \Bigg\{ \sum_{lnmpqr} a_{lnm} b_{pqr} \\ \times \Bigg[\langle \cos l\alpha_1 x \cos p\alpha_1 x \cos \kappa\alpha_1 x \rangle \left\langle \cos q\alpha_2 y \frac{\partial}{\partial y}(\cos n\alpha_2 y) \frac{\partial}{\partial y}(\cos \mu\alpha_2 y) \right\rangle \\ + \left\langle \cos p\alpha_1 x \frac{\partial}{\partial x}(\cos l\alpha_1 x) \frac{\partial}{\partial x}(\cos \kappa\alpha_1 x) \right\rangle \langle \cos q\alpha_2 y \cos n\alpha_2 y \cos \mu\alpha_2 y \rangle \Bigg] \\ \times g_m''(\pm\tfrac{1}{2}) r\pi (\mp 1)^r + \sum_{lnmpqr} c_{lnm} b_{pqr} (\pm)^{r+m} mr\pi^2 \\ \times \Bigg[\left\langle \sin l\alpha_1 x \frac{\partial}{\partial x}(\cos p\alpha_1 x) \cos \kappa\alpha_1 x \right\rangle \left\langle \sin n\alpha_2 y \sin q\alpha_2 y \frac{\partial}{\partial y}(\cos \mu\alpha_2 y) \right\rangle \\ - \left\langle \sin l\alpha_1 x \cos p\alpha_1 x \frac{\partial}{\partial x}(\cos \kappa\alpha_1 x) \right\rangle \left\langle \sin n\alpha_2 y \frac{\partial}{\partial y}(\cos q\alpha_2 y) \cos \mu\alpha_2 y \right\rangle \Bigg] \Bigg\}. \end{aligned} \tag{4.3}$$

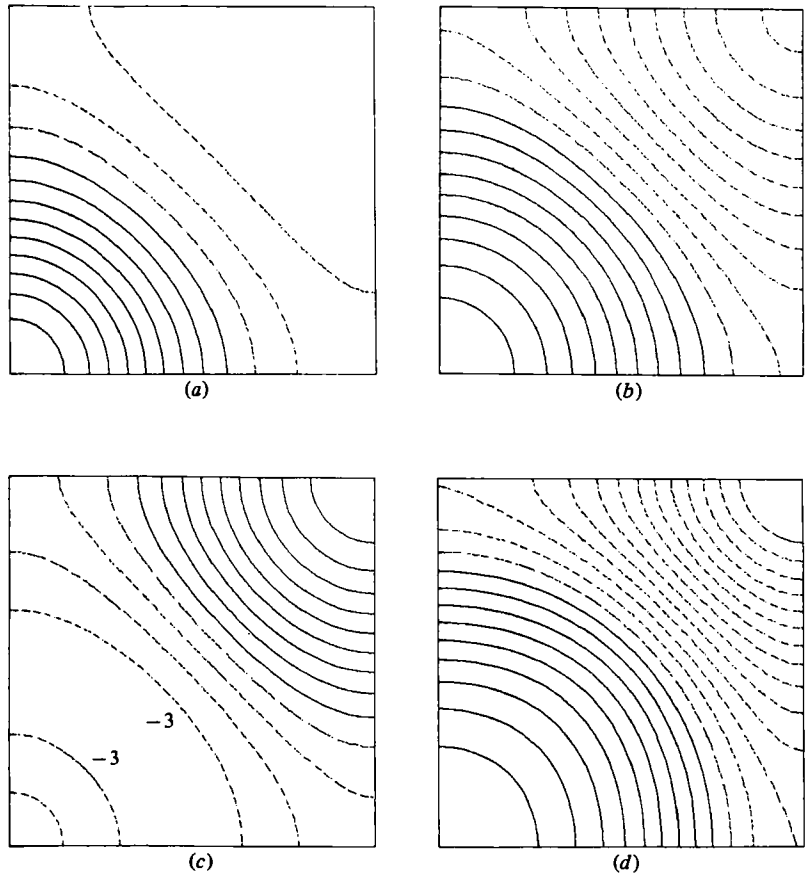

FIGURE 5. The dynamic pressure field at the lower (a, c) and at the upper (b, d) boundary. The cases $R = 1450$, $r = 21$ and $R = 5000$, $r = 11$ are shown in the upper and lower graphs respectively. The lines show levels of constant pressure corresponding to $0.1np_{\max}$, $n = 9, 8, \ldots$. The maximum values $p_{\max}$ of p are 60.9, 130.4, 303, 339 in (a), (b), (c), (d) respectively. In (c) n has been indicated where the sequence of level lines reverses.

The angular brackets indicate the average over the fluid layer, and g_m'' stands for the second derivative of the function g_m. Some examples of the function p are shown in figure 5.

The pressure distribution at the upper boundary corresponds closely to that expected in a fluid of constant viscosity. Since the viscosity at the upper surface is high, the variations introduced by the temperature dependence of the viscosity have a relatively small effect. Figures 5(b, d) are thus nearly indistinguishable from the graphs for a constant-viscosity fluid except for more pronounced asymmetry between positive and negative pressure values. Near the lower boundary, however, the viscosity variation plays a much more important role because of the low value of the viscosity at $z = -\frac{1}{2}$. In the case of a constant-viscosity fluid, $\eta = 0$, the relationship $p(\pi/\alpha - x, \pi/\alpha - y, -\frac{1}{2}) = p(x, y, \frac{1}{2})$ holds, and in the limit of small amplitude of convection the relationship $p(x, y, -\frac{1}{2}) = -p(x, y, \frac{1}{2})$ is approached. Figure 5(a) shows that a temperature-dependent viscosity can have a dramatic effect on the pressure distribution. Instead of the opposite sign for p at the lower boundary, we find that

the pressure field exhibits the same sign nearly everywhere on both boundaries as a function of x and y. In contrast with the hot rising plume near $x = y = 0$, which requires little work against viscous friction, the cold descending fluid does not have the excess buoyancy needed to build up a high-pressure region at the lower boundary. Figure 5(*a*) thus exhibits a plateau of negative p and a rise of the pressure towards the corner $x = y = 0$ which balances the suction provided by the rising hot fluid. This latter effect is still noticeable at higher Rayleigh number and lower viscosity ratio r as shown in figure 5(*c*), where the pressure also rises toward $x = y = 0$ even though it exhibits a sign opposite to that at the upper boundary area.

The pressure distribution at the boundaries of the convection layer is important in the theory of convection in the Earth's mantle, since it determines the distortion of the boundary. For a thin solid, but flexible, plate as boundary, an expression for the non-dimensional deflection ζ can easily be derived from the continuity of the normal stress across the boundary. Since the velocity vector vanishes at the boundary the deflection is directly proportional to p:

$$\zeta = p\nu\kappa/gd^3. \tag{4.4}$$

McKenzie (1977) considered the problem of two-dimensional convection with temperature-dependent viscosity in the case of stress-free boundaries. He also found a reversal of the sign of dynamic pressure at the boundary for strongly temperature-dependent viscosity.

5. Stability analysis

The stability of the steady solutions of the form (2.9) can be investigated by superimposing infinitesimal disturbances $\tilde{\phi}, \tilde{\psi}, \tilde{\theta}$ with an exponential time dependence $\exp\{\sigma t\}$. The general linear equations for the disturbances are given by

$$0 = \delta_i[(1+\eta z)\,\partial_k\partial_k\delta_i\tilde{\phi} + \eta\lambda_k\,\partial_k\delta_i\tilde{\phi}] + \delta_i\lambda_i\tilde{\theta}$$
$$-\delta_i\partial_j\left\{\frac{\eta\tilde{\theta}}{R}[\partial_j(\delta_i\phi+\varepsilon_i\psi)+\partial_i(\delta_j\phi+\varepsilon_j\psi)] + \frac{\eta\theta}{R}[\partial_j(\delta_i\tilde{\phi}+\varepsilon_i\tilde{\psi})+\partial_j(\delta_j\tilde{\phi}+\varepsilon_j\tilde{\psi})]\right\}, \tag{5.1a}$$

$$0 = [(1+\eta z)\,\partial_k\partial_k + \eta\lambda_k\,\partial_k]\varepsilon_j\varepsilon_j\tilde{\psi} - \varepsilon_i\partial_j\left\{\frac{\eta\tilde{\theta}}{R}[\partial_j(\delta_i\phi+\varepsilon_i\psi)+\partial_i(\delta_j\phi+\varepsilon_j\psi)]\right.$$
$$\left. + \frac{\eta\theta}{R}[\partial_j(\delta_i\tilde{\phi}+\varepsilon_i\tilde{\psi})+\partial_i(\delta_j\tilde{\phi}+\varepsilon_j\tilde{\psi})]\right\}, \tag{5.1b}$$

$$0 = \partial_j\partial_j\tilde{\theta} + R\lambda_j\delta_j\tilde{\phi} - (\delta_j\tilde{\phi}+\varepsilon_j\tilde{\psi})\,\partial_j\theta - (\delta_j\phi+\varepsilon_j\psi)\,\partial_j\tilde{\theta} - \sigma\tilde{\theta}. \tag{5.1c}$$

After expressions (2.9) for the steady solutions have been inserted, general solutions of (5.1) can be obtained in the form

$$\tilde{\phi} = \sum_{lnm} \tilde{a}_{lnm} \exp\{\mathrm{i}(l\alpha_1 x + n\alpha_2 y)\} g_m(z) \exp\{\mathrm{i}dx + \mathrm{i}by + \sigma t\}, \tag{5.2a}$$

$$\tilde{\psi} = \sum_{lnm} \tilde{c}_{lnm} \exp\{\mathrm{i}(l\alpha_1 x + n\alpha_2 y)\} f_m(z) \exp\{\mathrm{i}dx + \mathrm{i}by + \sigma t\}, \tag{5.2b}$$

$$\tilde{\theta} = \sum_{lnm} \tilde{b}_{lnm} \exp\{\mathrm{i}(l\alpha_1 x + n\alpha_2 y)\} f_m(z) \exp\{\mathrm{i}dx + \mathrm{i}by + \sigma t\}, \tag{5.2c}$$

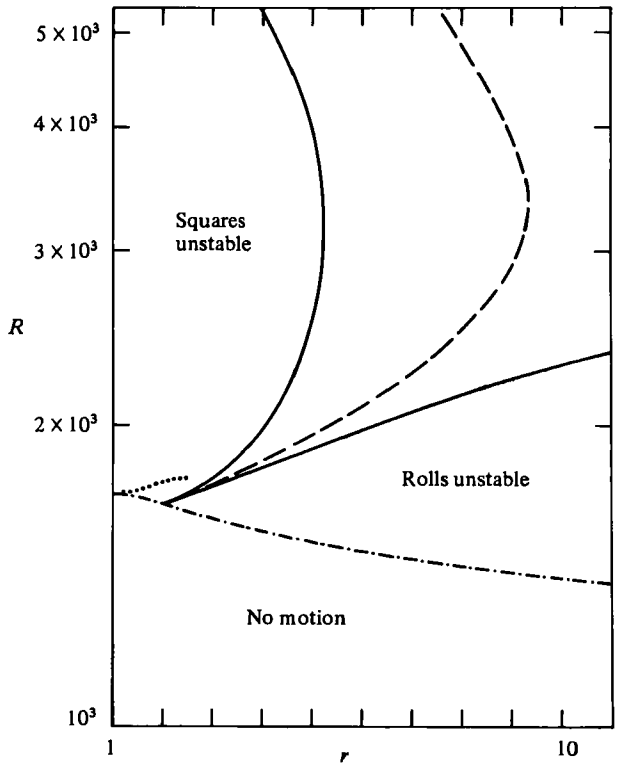

FIGURE 6. Stability regions of rolls and square-cell convection as functions of the Rayleigh number R and the viscosity ratio r. In the intermediate region both rolls and square cells are stable with respect to disturbances fitting the square lattice. The dashed line inside this region indicates the position where the (negative) growth rates of the strongest-growing disturbances for both forms of convection are equal. The dash–dotted curve indicates the critical Rayleigh number. Rolls are unstable below the dotted line according to (5.3).

where the summation indices l and n run through negative as well as positive integers, in contrast with (2.9). The wavenumbers d and b are the two Floquet parameters of the problem.

The general problem posed by (5.1) will not be investigated here. From the work of Schlüter, Lortz & Busse (1965) it is known that square cells are unstable near the critical value of the Rayleigh number in the case of a constant-viscosity fluid. In this instability one of the two rolls, that superimposed at right-angles form the square-pattern structure, grows while the other decays. This instability continues to occur when the Rayleigh number is increased, although the final state to which the unstable initial solution evolves is a form of bimodal convection once R exceeds a value of order 2×10^4 (Frick *et al.* 1983). In the present analysis we restrict attention to this instability by assuming the special case $b = d = 0$ of the representation (5.2) and by requiring that the disturbances have the same symmetry as the steady solution (2.9).

The analysis of the stability of two-dimensional convection rolls leads to a much simpler form of the disturbances than the representation (5.1). Only a single wavenumber in the third dimension has to be considered, and only a single Floquet parameter is required. Assuming that the roll solution depends on x, we find that the

most general form of disturbance is given by the representation (5.2) in which all coefficients with a subscript n different from unity are neglected.

The main results of the stability analysis are shown in figure 6. The square-cell solution becomes stable as r increases, and the roll solution becomes unstable when r increases even further. Only at the critical Rayleigh number at about $r = 2.0$ do the two stability boundaries converge. There is thus a region in (r, R)-space where both solutions are stable. This finding agrees well with the observed coexistence of rolls and square cells in the experimental realizations of the problem. The dashed line in figure 5 indicates the points at which the maximum growth rates of the disturbances for rolls and square cells are equal. It thus separates a region to the right where square cells can be regarded as the preferred solution from the region on the left where rolls are preferred.

The stability analysis is incomplete mainly because disturbances leading to a hexagonal pattern of convection have not been considered. For small viscosity variations analytical expressions for the Rayleigh number below which rolls are unstable with respect to hexagonal disturbances have been given by Busse (1967) and Palm, Ellingsen & Gjevik (1967). If we identify the parameter γ_2 of Busse (1967) with $-\eta$ according to relationships (2.1), (2.7), we obtain as expression of the stability boundary R_h below which rolls become unstable to hexagonal disturbances

$$R_h - R_0 = 660\frac{(r-1)^2}{(r+1)^2}. \tag{5.3}$$

But this expression is not meaningful outside the range of validity of the perturbation theory, $|r-1| \ll 1$, and is given here only as a rough guess.

It is worth noting that the point $r \approx 2.0$ at the critical Rayleigh number where the stability boundaries for square cells and rolls meet corresponds to the point where the convective heat transport of these two solutions becomes equal. This property is a consequence of the extremum principle of Busse (1967) applied to the present case and agrees with numerical results obtained for low values of $R - R_c$.

6. Concluding remarks

The replacement by square cells of rolls as the preferred form of convection for increasing viscosity ratio r is in many respects similar to the replacement of rolls by hexagonal cells. In a sense square cells may be regarded as 'superhexagons'. Because the ratio of boundary area to volume is larger for a square cell than for a hexagonal cell, the former configuration offers better possibilities for asymmetries. By minimizing the shear in the highly viscous region of descending flow and concentrating the rising motion in a plume of low-viscosity fluid, square-cell convection appears to be even more effective than hexagonal convection in decreasing viscous dissipation. In contrast with hexagonal motion, the asymmetric square cell cannot be formed by the superposition of waves with equal horizontal wave vectors of equal length. The configuration of the asymmetric square cell is produced in first approximation by the superposition of the terms proportional to $\cos\alpha(x+y)$, $\cos\alpha(x-y)$ onto the fundamental terms proportional to $\cos\alpha x$ and $\cos\alpha y$ in the representation (2.9). Nonlinear interactions of higher order than in the case of hexagonal convection are thus required to establish square cells as the preferred form of convection. This property becomes evident when the expansion of the Rayleigh number in powers of the amplitude ϵ of convection is considered, $R = R_c + \epsilon R_1 + \epsilon^2 R_2 + \ldots$. In contrast with

the hexagonal solution the coefficient R_1 always vanishes for the square-cell solution as it does in the case of rolls.

Oliver (1980) has attempted a preliminary analysis of (2.2) in terms of such an expansion. His results indicate that the coefficient R_2 may become negative for an exponential dependence of the viscosity of temperature, which would imply subcritical finite-amplitude convection (Oliver, private communication). The present computations have not shown this effect at viscosity ratios r of order ten. But these ratios are smaller than those typically considered by Oliver, and the difference in the viscosity functions may be another reason for the absence of subcritical finite-amplitude square-cell convection.

Experimental measurements of the Nusselt number near the critical Rayleigh number (Stengel *et al.* 1982; Richter, Nataf & Daly 1983) show that subcritical finite-amplitude convection is an important effect. But at low and moderate values of the viscosity ratio r subcritical convection occurs in the form of hexagonal cells. As the Rayleigh number is increased, these cells change into square cells if the viscosity ratio is sufficiently large. We conclude that the stability of square cells is not connected with the existence of subcritical finite-amplitude solutions as in the case of hexagonal cells. This conclusion does not preclude the existence and possible experimental realization of subcritical square-cell convection at large viscosity ratios r.

The research reported in this paper has been supported by the Geophysics Section of the U.S. National Science Foundation. The authors are indebted to the College of Letters and Sciences, UCLA, for the allocation of computing resources.

Note added in proof. We would like to use this opportunity to point out an error of interpretation in the paper by Frick *et al.* (1983). The two surfaces shown in figure 6 of the paper actually coincide. There is thus for given values α_1, α_2, and R only one solution of the square pattern type. We are grateful to Dr J. W. Swift for bringing this point to our attention. We also note that $\alpha_2 = 410$ in table 1 should be replaced by $\alpha_2 = 4.0$.

REFERENCES

BOOKER, J. R. 1976 Thermal convection with strongly temperature-dependent viscosity. *J. Fluid Mech.* **76**, 741–754.

BUSSE, F. H. 1962 Das Stabilitätsverhalten der Zellularkonvektion bei endlicher Amplitude. Dissertation, University of Munich. [English transl. by S. H. Davis, *Rand Rep.* LT-66-19, *Rand Corp., Santa Monica, California.*]

BUSSE, F. H. 1967 The stability of finite amplitude cellular convection and its relation to an extremum principle. *J. Fluid Mech.* **30**, 625–649.

BUSSE, F. H. & WHITEHEAD, J. A. 1971 Instabilities of convection rolls in a high Prandtl number fluid. *J. Fluid Mech.* **47**, 305–320.

CHANDRASEKHAR, S. 1961 *Hydrodynamic and Hydromagnetic Stability.* Clarendon.

DEBREMAECKER, J.-C. 1977 Convection in the Earth's mantle. *Tectonophys.* **41**, 195–208.

FOSTER, T. D. 1969 Convection in a variable viscosity fluid heated from within. *J. Geophys. Res.* **74**, 685–593.

FRICK, H., BUSSE, F. H. & CLEVER, R. M. 1983 Steady three-dimensional convection at high Prandtl number. *J. Fluid Mech.* **127**, 141–153.

HOUSTON, M. H. & DEBREMAECKER, J.-C. 1975 Numerical models of convection in the upper mantle. *J. Geophys. Res.* **80**, 742–751.

HOARD, C. Q., ROBERTSON, C. R. & ACRIVOS, A. 1970 Experiments on the cellular structure of Bénard convection. *Intl J. Heat Mass Transfer* **13**, 849–855.

JACOBY, W. R. & SCHMELING, H. 1982 On the effects of the lithosphere on mantle convection and evolution. *Phys. Earth Planet. Interiors* **29**, 305–319.

KOPITZKE, V. 1979 Finite element convection models: comparison of shallow and deep mantle convection, and temperature in the mantle. *J. Geophys.* **46**, 97–121.

MCKENZIE, D. 1977 Surface deformation, gravity anomalies and convection. *Geophys. J. R. Astron. Soc.* **48**, 211–238.

OLIVER, D. S. 1980 Bénard convection with strongly temperature-dependent viscosity. Ph.D. dissertation, University of Washington.

OLIVER, D. S. & BOOKER, J. R. 1983 Planform of convection with strongly temperature-dependent viscosity. *Geophys. Astrophys. Fluid Dyn.* **27**, 73–85.

PALM, E. 1960 On the tendency towards hexagonal cells in steady convection. *J. Fluid Mech.* **8**, 183–192.

PALM, E., ELLINGSEN, T. & GJEVIK, B. 1967 On the occurrence of cellular motion in Bénard convection. *J. Fluid Mech.* **30**, 651–661.

RICHTER, F. M. 1978 Experiments on the stability of convection rolls in fluids whose viscosity depends on temperature. *J. Fluid Mech.* **89**, 553–560.

RICHTER, F. M., NATAF, H.-C. & DALY, S. F. 1983 Heat transfer and horizontally averaged temperature of convection with large viscosity variations. *J. Fluid Mech.* **129**, 173–192.

ROBINSON, J. L. 1965 A boundary layer convection cell. *Woods Hole Ocenogr. Inst. Rep.* 65-51, pp. 92–112.

SCHLÜTER, A., LORTZ, D. & BUSSE, F. 1965 On the stability of steady finite amplitude convection. *J. Fluid Mech.* **23**, 129–144.

SCHMELING, H. & JACOBY, W. R. 1981 On modelling the lithosphere in mantle convection. *J. Geophys.* **50**, 89–100.

SEGEL, L. A. & STUART, J. T. 1962 On the question of the preferred mode in cellular thermal convection. *J. Fluid Mech.* **13**, 289–306.

SILVESTON, P. L. 1958 Wärmedurchgang in waagerechten Flüssigkeitsschichten. *Forsch. Ing. Wes.* **24**, 29–32, 59–69.

SOMERSCALES, E. F. C. & DOUGHERTY, T. S. 1970 Observed flow patterns at the initiation of convection in a horizontal liquid layer heated from below. *J. Fluid Mech.* **42**, 755–768.

STENGEL, K. C., OLIVER, D. S. & BOOKER, J. R. 1982 Onset of convection in a variable-viscosity fluid. *J. Fluid Mech.* **120**, 411–431.

TIPPELSKIRCH, H. 1956 Über Konvektionszellen, insbesondere in flüssigem Schwefel. *Beitr. Phys. Atmos.* **29**, 37–54.

TORRANCE, K. E. & TURCOTTE, D. L. 1971 Thermal convection with large viscosity variations. *J. Fluid Mech.* **47**, 113–125.

TOZER, D. C. 1967 Towards a theory of thermal convection in the mantle. In *The Earth's Mantle* (ed. T. F. Gaskell), pp. 325–353. Academic.

WALDEN, R. W. & AHLERS, G. 1981 Non-Boussinesq and penetrative convection in a cylindrical cell. *J. Fluid Mech.* **109**, 89–114.

WHITE, D. 1984 The planforms and onset of convection with a temperature-dependent viscosity. *J. Fluid Mech.* (to be published).